

DFTT 16/2001
INFNCA-TH0105
IPPP/01/25
DCPT/01/50

Weak interactions in polarized semi-inclusive DIS

M. Anselmino¹, M. Boglione², U. D'Alesio³, F. Murgia³

¹ Dipartimento di Fisica Teorica, Università di Torino and
INFN, Sezione di Torino, Via P. Giuria 1, I-10125 Torino, Italy

² Department of Physics, University of Durham, Science Laboratories
South Road, Durham DH11 3LE, United Kingdom

³ INFN, Sezione di Cagliari and Dipartimento di Fisica, Università di Cagliari,
C.P. 170, I-09042 Monserrato (CA), Italy

Abstract

We calculate, within pQCD parton model at leading orders, the expression of the polarization P of spin 1/2 hadrons (typically baryons), produced in polarized semi-inclusive DIS in all possible cases in which weak interactions are involved. We discuss how to gather new information on fragmentation and distribution functions and give numerical estimates in the cases for which data are or will soon be available.

PACS numbers: 13.60.Hb, 13.85.Ni, 13.87.Fh, 13.88.+e

1. Introduction

The polarization of spin 1/2 baryons inclusively produced in polarized Deep Inelastic Scattering processes may be useful, if measurable, to obtain new information on polarized distribution and fragmentation functions. A lot of attention has recently been dedicated to the self-revealing polarization of Λ 's and other hyperons [1]-[12]. Most papers, with the exception of Refs. [5], [8] and [11], do not consider weak interaction contributions, due to lack of available experimental information.

NOMAD collaboration have recently published some very interesting results [13] on the polarization in charged current interactions; more data might soon be available from high energy neutral current processes at HERA, due to electro-weak interference effects. It is then appropriate and timely to perform a systematic and comprehensive study of weak interaction contributions to the production and the polarization of baryons in as many as possible DIS processes. We stress that such contributions are an important source of new information, due to the natural neutrino polarization and to the selected couplings of W 's to pure helicity states.

We consider weak interactions in the following processes:

$$\begin{aligned}
 p & \rightarrow \nu + X && \text{(charged current)} \\
 p & \rightarrow \nu^+ + X && \text{(charged current)} \\
 \nu p & \rightarrow \nu + X && \text{(charged current)} \\
 \nu^+ p & \rightarrow \nu + X && \text{(charged current)} \\
 p & \rightarrow \nu + X && \text{(neutral current)} \\
 p & \rightarrow \nu + X && \text{(neutral current)} \\
 \nu p & \rightarrow \nu + X && \text{(neutral current)}
 \end{aligned}$$

where the lepton ν and the proton p may or may not be polarized, whereas the neutrinos are obviously always polarized ($\lambda = \pm 1/2$, $\lambda = \pm 1/2$).

In our calculations we take into account leading twist factorization theorem, Standard Model elementary interactions at lowest perturbative order and LO QCD evolution only. Consequently the cross-sections for the production of a hadron B in the current fragmentation region are given by

$$\frac{d}{dx dy dz} = \sum_q^X q(x; Q^2) \frac{d}{dy} D_{B=q}(z; Q^2); \quad (1)$$

where $q(x; Q^2)$ is the quark q distribution function, $D_{B=q}(z; Q^2)$ is the fragmentation function of the quark into the detected hadron B , and $d^4 = dy$ is the elementary cross-section. The usual DIS variables x , y and z are defined as $x = Q^2 = 2p \cdot q$, $y = q \cdot p / p \cdot q$ and $z = p_B \cdot p / p \cdot q$ (see also Appendix B).

In Sections 2-4 we consider separately the different processes, and derive explicit expressions for the polarization of a neutral baryon B in terms of elementary dynamics, quark distribution and fragmentation functions. In Section 5 we discuss how experimental data could be used to obtain specific new information and give predictions

for several processes which might be of interest in the near future. In Appendix A we give full information on the kinematical ranges and configurations for each of the experiments in progress or planned, used to derive our numerical results. In Appendix B we discuss mass effects in the fragmentation process, to clarify differences and relationships between different definitions of the variable on which the fragmentation functions depend.

2. Charged current processes, $p \rightarrow \nu X$ and $\bar{p} \rightarrow \bar{\nu} X$

Let us consider first the neutrino initiated processes, $p \rightarrow \nu X$; for them, there exist 4 possible elementary contributions, corresponding to the interactions:

$$\begin{aligned} d_j &\rightarrow \nu u_i \\ u_i &\rightarrow \nu d_j \\ u_i &\rightarrow \bar{\nu} d_j \\ d_j &\rightarrow \bar{\nu} u_i \end{aligned} \quad (2)$$

where we use the notation

$$u_i = u; c \quad d_j = d; s : \quad (3)$$

Neglecting quark masses one finds that there is only one non-zero helicity amplitude $\hat{M}_{q_i; q_j}^{\nu; \bar{\nu}}$ for each of the elementary processes in (2), and precisely

$$\hat{M}_{q_i; q_j}^{\nu; \bar{\nu}} = \hat{M}_{++; ++}^{\nu; \bar{\nu}} = \frac{4}{\sin^2 \theta_w} \frac{V_{ij}}{y + M_W^2 = xs} ; \quad (4)$$

$$\hat{M}_{q_i; q_j}^{\bar{\nu}; \nu} = \hat{M}_{+; +}^{\bar{\nu}; \nu} = \frac{4}{\sin^2 \theta_w} \frac{V_{ij}}{y + M_W^2 = xs} \frac{y}{y + M_W^2 = xs} ; \quad (5)$$

where, according to usual SM rules,

$$V_{ud} = V_{cs} = \cos \theta_c \quad V_{us} = V_{cd} = \sin \theta_c ; \quad (6)$$

θ_w is the Weinberg angle, θ_c is the Cabibbo angle and $V_{ij} = V_{ji}$.

The elementary cross-sections are computed according to

$$\frac{d\hat{\sigma}_0}{dQ^2} = \frac{1}{16 x^2 s^2} \mathcal{J} \hat{M}_{0; 0}^2 = \frac{1}{sx} \frac{d\hat{\sigma}_0}{dy} ; \quad (7)$$

from which we obtain

$$\frac{d\hat{\sigma}_{d_j \rightarrow \nu u_i}}{dy} = \frac{d\hat{\sigma}_{++}^{\nu; \bar{\nu}}}{dy} = \frac{2}{xs} \frac{\mathcal{J}_{ij}^2}{\sin^4 \theta_w} \frac{1}{y + M_W^2 = xs} ; \quad (8)$$

$$\frac{d\hat{\sigma}_{u_i \rightarrow \nu d_j}}{dy} = \frac{d\hat{\sigma}_{+}^{\bar{\nu}; \nu}}{dy} = \frac{2}{xs} \frac{\mathcal{J}_{ij}^2}{\sin^4 \theta_w} \frac{1}{y + M_W^2 = xs} \frac{y}{y + M_W^2 = xs} ; \quad (9)$$

Notice that both γ_5 and $\gamma_5 \gamma_3$ couple only to quarks with negative helicity and antiquarks with positive helicity.

We can now compute the longitudinal polarizations $P_{[\lambda; \gamma]}(B)$ and $P_{[\lambda; \gamma]}(B)$ for any spin $1=2$ baryon B (Λ 's and Σ 's for instance) produced in neutrino initiated, charged current DIS scattering processes:

$$P_{[\lambda; \gamma]}(B) = \frac{d_{p!}^{-\lambda} \gamma_5 \gamma_3 \cdot B+X \quad d_{p!}^{-\lambda} \gamma_5 \gamma_3 \cdot B-X}{d_{p!}^{-\lambda} \gamma_5 \gamma_3 \cdot B+X + d_{p!}^{-\lambda} \gamma_5 \gamma_3 \cdot B-X} \quad (10)$$

and

$$P_{[\lambda; \gamma]}(B) = \frac{d_{p!}^{-\lambda} \gamma_5 \gamma_3 \cdot B+X \quad d_{p!}^{-\lambda} \gamma_5 \gamma_3 \cdot B-X}{d_{p!}^{-\lambda} \gamma_5 \gamma_3 \cdot B+X + d_{p!}^{-\lambda} \gamma_5 \gamma_3 \cdot B-X}; \quad (11)$$

where B denotes a baryon B with helicity λ .

In the most general case, when also the proton p is polarized λ and we denote by an apex S its spin state λ from Eqs. (1), (10) and (11) we obtain:

$$P_{[\lambda; \gamma]}^{(S)}(B) = \frac{P_{i;j}^{(S)} [(d_j)^{(S)} d^{+\lambda d_j!} u_i D_{B=u_i} \quad (u_i)^{(S)} d^{+\lambda u_i!} d_j D_{B=d_j}]}{P_{i;j}^{(S)} [(d_j)^{(S)} d^{+\lambda d_j!} u_i D_{B=u_i} + (u_i)^{(S)} d^{+\lambda u_i!} d_j D_{B=d_j}]} \quad (12)$$

and

$$P_{[\lambda; \gamma]}^{(S)}(B) = \frac{P_{i;j}^{(S)} [(u_i)^{(S)} d^{+\lambda u_i!} d_j D_{B=d_j} \quad (d_j)^{(S)} d^{+\lambda d_j!} u_i D_{B=u_i}]}{[(u_i)^{(S)} d^{+\lambda u_i!} d_j D_{B=d_j} + (d_j)^{(S)} d^{+\lambda d_j!} u_i D_{B=u_i}]}; \quad (13)$$

where an expression like $(q)^{(S)}$ stands for the number density (distribution function) of quarks q with helicity λ inside a proton with spin S , whereas q alone refers, as usual, to a proton with $+$ helicity. The polarized fragmentation functions are defined as

$$D_{B=q} \quad D_{B+=q_+} \quad D_{B-=q_-} = D_{B=q} \quad D_{B+=q} : \quad (14)$$

If we now explicitly perform the sum over flavours in the numerators and denominators of Eqs. (12) and (13), neglecting c quark contributions, and use Eqs. (8) and (9), we obtain for longitudinally (λ helicity) polarized protons

$$P_{[\lambda; \gamma]}^{(\lambda)}(B; x; y; z) = \frac{[d + R s] D_{B=u} \quad (1 - \gamma^2) u [D_{B=d} + R D_{B=s}]}{[d + R s] D_{B=u} + (1 - \gamma^2) u [D_{B=d} + R D_{B=s}]} \quad (15)$$

and

$$P_{[\lambda; \gamma]}^{(\lambda)}(B; x; y; z) = \frac{[d + R s] D_{B=u} \quad (1 - \gamma^2) u [D_{B=d} + R D_{B=s}]}{[d + R s] D_{B=u} + (1 - \gamma^2) u [D_{B=d} + R D_{B=s}]}; \quad (16)$$

where $R = \sin^2 \theta_c = \cos^2 \theta_c \approx 0.056$.

In the simpler case in which the proton is unpolarized one replaces q_+ and q_- with $q=2$ so that Eqs. (15) and (16) become respectively

$$P_{[\lambda; \gamma]}^{(0)}(B; x; y; z) = \frac{[d + R s] D_{B=u} \quad (1 - \gamma^2) u [D_{B=d} + R D_{B=s}]}{[d + R s] D_{B=u} + (1 - \gamma^2) u [D_{B=d} + R D_{B=s}]} \quad (17)$$

and

$$P_{[;']}^{(0)}(B; \mathbf{x}; \mathbf{y}; z) = \frac{[d + R s] D_{B=u} (1 - y^2) u [D_{B=d} + R D_{B=s}]}{[d + R s] D_{B=u} + (1 - y^2) u [D_{B=d} + R D_{B=s}]} ; \quad (18)$$

in agreement with the results of Ref. [11].

The formulae given above hold for any baryon and antibaryon with spin 1=2. If we specify the final hadron observed, further simplifications are possible. Let's consider the case in which a baryon is produced, or, in general, a baryon (rather than an antibaryon): in this case we can neglect terms which contain both q distributions (in a proton) and q fragmentations (into a \bar{q}) as they are both small, in particular at large x and z . Then we simply have:

$$P_{[;']}^{(+)}(\bar{q}; z) = P_{[;']}^{(0)}(\bar{q}; z) = \frac{D_{=u}}{D_{=u}} ; \quad (19)$$

$$P_{[;']}^{(+)}(q; z) = P_{[;']}^{(0)}(q; z) = \frac{D_{=d} + R D_{=s}}{D_{=d} + R D_{=s}} ; \quad (20)$$

and the polarizations, up to QCD evolution effects, become functions of the variable z only, since any other term apart from the fragmentation functions cancels out. For Eq. (20) to hold one should also avoid large y regions, due to the factor $(1 - y^2)$ in Eq. (18).

Eqs. (19) and (20) relate the values of the longitudinal polarization $P^{(+)}$ to a quantity with a clear physical meaning, i.e. the ratio $D_{=q} = D_{=q}$; this happens with weak charged current interactions { while it cannot happen in purely electromagnetic DIS [12] { due to the selection of the quark helicity and flavour in the coupling with neutrinos. A measurement of $P^{(+)}$ offers new direct information on the fragmentation process. We shall discuss further this point in Section 5.

Similar results hold for the \bar{p} ! "X processes; the contributing elementary interactions are:

$$\begin{aligned} & \bar{u}_i ! d_j \\ & \bar{d}_j ! u_i \\ & \bar{d}_j ! u_i \\ & \bar{u}_i ! d_j \end{aligned} \quad (21)$$

with the same cross-sections as those computed in Eqs. (8) and (9):

$$\frac{d^{\bar{u}_i ! d_j}}{dy} = \frac{d^{\bar{u}_i ! d_j}}{dy} = \frac{d^{\bar{d}_j ! u_i}}{dy} = \frac{d^{\bar{d}_j ! u_i}}{dy} ; \quad (22)$$

$$\frac{d^{\bar{d}_j ! u_i}}{dy} = \frac{d^{\bar{d}_j ! u_i}}{dy} = \frac{d^{\bar{u}_i ! d_j}}{dy} = \frac{d^{\bar{u}_i ! d_j}}{dy} \quad (23)$$

The analogue of Eqs. (15) and (16) is now

$$P_{[\uparrow; \downarrow]}^{(\)}(B; x; y; z) = \frac{(1-y)^2 [d + R s] D_{B=u} + u [D_{B=d} + R D_{B=s}]}{(1-y)^2 [d + R s] D_{B=u} + u [D_{B=d} + R D_{B=s}]} \quad (24)$$

and

$$P_{[\downarrow; \uparrow]}^{(\)}(B; x; y; z) = \frac{(1-y)^2 [d + R s] D_{B=u} + u [D_{B=d} + R D_{B=s}]}{(1-y)^2 [d + R s] D_{B=u} + u [D_{B=d} + R D_{B=s}]} \quad (25)$$

and similarly for the analogue of Eqs. (17) and (18) (one simply replaces in the above equations the quark and antiquark helicity distributions with the unpolarized ones).

In the case in which one can neglect antiquark contributions (as for 's) one has again, as in Eqs. (19) and (20),

$$P_{[\uparrow; \downarrow]}^{(\)}(\ ; z) = P_{[\downarrow; \uparrow]}^{(0)}(\ ; z) = \frac{D_{=d} + R D_{=s}}{D_{=d} + R D_{=s}}; \quad (26)$$

$$P_{[\downarrow; \uparrow]}^{(\)}(\ ; z) = P_{[\uparrow; \downarrow]}^{(0)}(\ ; z) = \frac{D_{=u}}{D_{=u}} \quad (27)$$

3. Neutral current neutrino processes, $p \rightarrow \nu X$

There are 4 different kinds of elementary interactions contributing to these processes

$$\begin{array}{l} q \rightarrow q \\ q \rightarrow q \\ q \rightarrow q \\ q \rightarrow q \end{array} \quad (28)$$

where q can be either u_j or d_j .

There are 2 non-zero independent helicity amplitudes for each process in (28). These lead, through Eq. (7), to the following elementary cross-sections

$$\begin{aligned} \frac{d\hat{\sigma}_+^{q!q}}{dy} &= \frac{d\hat{\sigma}_+^{q!q}}{dy} = \frac{2 (2e_q \sin^2 \theta_w)^2}{4xs \sin^4 \theta_w \cos^4 \theta_w} \frac{1-y}{y + M_Z^2/xs} ; \\ \frac{d\hat{\sigma}_+^{q!q}}{dy} &= \frac{d\hat{\sigma}_{++}^{q!q}}{dy} = \frac{2 (1 - 2j_q \sin^2 \theta_w)^2}{4xs \sin^4 \theta_w \cos^4 \theta_w} \frac{1}{y + M_Z^2/xs} ; \\ \frac{d\hat{\sigma}_+^{q!q}}{dy} &= \frac{d\hat{\sigma}_+^{q!q}}{dy} = \frac{2 (1 - 2j_q \sin^2 \theta_w)^2}{4xs \sin^4 \theta_w \cos^4 \theta_w} \frac{1-y}{y + M_Z^2/xs} ; \\ \frac{d\hat{\sigma}_+^{q!q}}{dy} &= \frac{d\hat{\sigma}_{++}^{q!q}}{dy} = \frac{2 (2e_q \sin^2 \theta_w)^2}{4xs \sin^4 \theta_w \cos^4 \theta_w} \frac{1}{y + M_Z^2/xs} ; \end{aligned} \quad (29)$$

where e_q is the quark charge in units of the proton charge.

In analogy to what we did in the previous paragraph, the longitudinal polarization of the produced baryon B is defined as

$$P_{[;]}(B) = \frac{d_{p! B+X} - d_{p! B-X}}{d_{p! B+X} + d_{p! B-X}} \quad (30)$$

and

$$P_{[;]}(B) = \frac{d_{p! B+X} - d_{p! B-X}}{d_{p! B+X} + d_{p! B-X}} \quad (31)$$

For the numerator and denominator of $P_{[;]}(B)$ and $P_{[;]}(B)$ separately, one obtains, for a generic spin state S of the proton:

$$\begin{aligned} N_{[;]}^{(S)}(B) = & \sum_j^{nh} (u_j)_+^{(S)} (1 - Y)^2 16C^2 + (u_j)^{(S)} (1 - 4C)^2 D_{B=u_j} \\ & + \sum_h (d_j)_+^{(S)} (1 - Y)^2 4C^2 + (d_j)^{(S)} (1 - 2C)^2 D_{B=d_j} \\ & + \sum_h (u_j)_+^{(S)} (1 - Y)^2 (1 - 4C)^2 + (u_j)^{(S)} 16C^2 D_{B=u_j} \\ & + \sum_h (d_j)_+^{(S)} (1 - Y)^2 (1 - 2C)^2 + (d_j)^{(S)} 4C^2 D_{B=d_j} ; \quad (32) \end{aligned}$$

$$\begin{aligned} D_{[;]}^{(S)}(B) = & \sum_j^{nh} (u_j)_+^{(S)} (1 - Y)^2 16C^2 + (u_j)^{(S)} (1 - 4C)^2 D_{B=u_j} \\ & + \sum_h (d_j)_+^{(S)} (1 - Y)^2 4C^2 + (d_j)^{(S)} (1 - 2C)^2 D_{B=d_j} \\ & + \sum_h (u_j)_+^{(S)} (1 - Y)^2 (1 - 4C)^2 + (u_j)^{(S)} 16C^2 D_{B=u_j} \\ & + \sum_h (d_j)_+^{(S)} (1 - Y)^2 (1 - 2C)^2 + (d_j)^{(S)} 4C^2 D_{B=d_j} ; \quad (33) \end{aligned}$$

and

$$\begin{aligned} N_{[;]}^{(S)}(B) = & \sum_j^{nh} (u_j)_+^{(S)} 16C^2 + (u_j)^{(S)} (1 - Y)^2 (1 - 4C)^2 D_{B=u_j} \\ & + \sum_h (d_j)_+^{(S)} 4C^2 + (d_j)^{(S)} (1 - Y)^2 (1 - 2C)^2 D_{B=d_j} \\ & + \sum_h (u_j)_+^{(S)} (1 - 4C)^2 + (u_j)^{(S)} (1 - Y)^2 16C^2 D_{B=u_j} \\ & + \sum_h (d_j)_+^{(S)} (1 - 2C)^2 + (d_j)^{(S)} (1 - Y)^2 4C^2 D_{B=d_j} ; \quad (34) \end{aligned}$$

$$\begin{aligned} D_{[;]}^{(S)}(B) = & \sum_j^{nh} (u_j)_+^{(S)} 16C^2 + (u_j)^{(S)} (1 - Y)^2 (1 - 4C)^2 D_{B=u_j} \\ & + \sum_h (d_j)_+^{(S)} 4C^2 + (d_j)^{(S)} (1 - Y)^2 (1 - 2C)^2 D_{B=d_j} \\ & + \sum_h (u_j)_+^{(S)} (1 - 4C)^2 + (u_j)^{(S)} (1 - Y)^2 16C^2 D_{B=u_j} \\ & + \sum_h (d_j)_+^{(S)} (1 - 2C)^2 + (d_j)^{(S)} (1 - Y)^2 4C^2 D_{B=d_j} ; \quad (35) \end{aligned}$$

where $C = \sin^2 \theta_w = 3$.

In the case of (or any baryon, rather than antibaryon) production, a simple expression for its longitudinal polarization P can be obtained by neglecting the antiquark contributions and the terms proportional to $\sin^4 \theta_w$. For longitudinally polarized protons in this approximation we have

$$P_{[;]}^{()} = \frac{P_j [(u_j) (1 - 8C) D_{=u_j} + (d_j) (1 - 4C) D_{=d_j}]}{P_j [(u_j) (1 - 8C) D_{=u_j} + (d_j) (1 - 4C) D_{=d_j}]}; \quad (36)$$

whereas for unpolarized proton, where $q = 2$, one obtains

$$P_{[;]}^{(0)} = \frac{P_j [u_j (1 - 8C) D_{=u_j} + d_j (1 - 4C) D_{=d_j}]}{P_j [u_j (1 - 8C) D_{=u_j} + d_j (1 - 4C) D_{=d_j}]} \quad (37)$$

Similar formulae, avoiding the large y region, hold for $P_{[;]}^{()}$ and for $P_{[;]}^{(0)}$.

4. Neutral current lepton processes, $\nu \rightarrow \nu' X$

The possible elementary scatterings contributing to this process are of the form

$$\nu q \rightarrow \nu' q \quad (38)$$

where ν can be either ν^+ or ν^- and q can be any quark or antiquark.

There are 4 non-zero independent helicity amplitudes corresponding to the process in (38). Notice that in this case we must take into account the contributions of both weak and electromagnetic interactions, and the amplitudes are given by the sum of the two corresponding terms. According to Eq. (7), the elementary cross-sections can be written as

$$\begin{aligned} \frac{d^{\nu q \rightarrow \nu' q}}{dy} &= \frac{2}{16xs} N^{\nu q} \frac{1}{y + M_Z^2 = xs} \frac{8e_q^2}{y}; \\ \frac{d^{\nu q \rightarrow \nu' q}}{dy} &= \frac{2}{16xs} N^{\nu q} \frac{1}{y + M_Z^2 = xs} \frac{8e_q^2}{y} (1 - y)^2; \end{aligned} \quad (39)$$

where again ν can be either ν^+ or ν^- , q can be any quark or antiquark $q = u_j; d_j$ and e_q is the quark charge. For the coefficients $N^{\nu q}$ we have ($C = \sin^2 \theta_w = 3$)

$$\begin{aligned} N_{++}^{\nu u_j} &= N_{+}^{\nu u_j} = N_{+}^{\nu' u_j} = N_{+}^{\nu' u_j} = \frac{16C}{1 - 3C}, \quad 1:60; \\ N_{+}^{\nu u_j} &= N_{++}^{\nu u_j} = N_{+}^{\nu' u_j} = N_{+}^{\nu' u_j} = \frac{4(1 - 4C)}{1 - 3C}, \quad 3:60; \\ N_{+}^{\nu u_j} &= N_{+}^{\nu u_j} = N_{++}^{\nu' u_j} = N_{+}^{\nu' u_j} = \frac{8(1 - 6C)}{3(1 - 3C)}, \quad 1:87; \\ N_{+}^{\nu u_j} &= N_{+}^{\nu u_j} = N_{+}^{\nu' u_j} = N_{++}^{\nu' u_j} = \frac{2(6C - 1)(1 - 4C)}{3C(1 - 3C)}, \quad 4:19; \end{aligned} \quad (40)$$

and

$$\begin{aligned}
 N_{++}^{\lambda d_j} &= N_{+}^{\lambda d_j} = N_{+}^{+\lambda d_j} = N_{+}^{-\lambda d_j} = \frac{8C}{1-3C}, \quad 0.80; \\
 N_{+}^{\lambda d_j} &= N_{++}^{\lambda d_j} = N_{+}^{+\lambda d_j} = N_{+}^{-\lambda d_j} = \frac{4(2C-1)}{1-3C}, \quad 4.40; \\
 N_{+}^{\lambda d_j} &= N_{+}^{\lambda d_j} = N_{++}^{+\lambda d_j} = N_{+}^{-\lambda d_j} = \frac{4(6C-1)}{3(1-3C)}, \quad 0.93; \\
 N_{+}^{\lambda d_j} &= N_{+}^{\lambda d_j} = N_{+}^{+\lambda d_j} = N_{++}^{-\lambda d_j} = \frac{2(1-6C)(1-2C)}{3C(1-3C)}, \quad 5.12; \quad (41)
 \end{aligned}$$

We can now proceed to the calculation of the longitudinal polarization P of the observed spin 1=2 baryon

$$P_{[\lambda;\lambda]}(B) = \frac{d_{\lambda\lambda}^{\lambda B+X} d_{\lambda\lambda}^{\lambda B-X}}{d_{\lambda\lambda}^{\lambda B+X} + d_{\lambda\lambda}^{\lambda B-X}}; \quad (42)$$

where λ can be either $+$ or $-$.

$P_{[\lambda;\lambda]}(B)$ can be evaluated for any lepton and proton spin configuration. When both the proton p and the lepton λ are longitudinally polarized (in helicity states), the polarization P becomes

$$P_{[\lambda;\lambda]}^{(;\lambda)}(B) = \frac{P_{\lambda}^h \sum_q q d_{++}^{\lambda q\lambda} d_{\lambda\lambda}^{\lambda q\lambda} D_{B=q}}{P_{\lambda}^h \sum_q q d_{++}^{\lambda q\lambda} d_{\lambda\lambda}^{\lambda q\lambda} D_{B=q}}; \quad (43)$$

where again λ stands for either $+$ or $-$, and the sum runs over all quarks and antiquarks, $q = u; d; s; \bar{u}; \bar{d}; \bar{s}; \dots$.

For longitudinally polarized leptons but unpolarized protons ($q \neq q=2$) we have

$$P_{[\lambda;\lambda]}^{(;\lambda)} = \frac{P_{\lambda}^h \sum_q q d_{++}^{\lambda q\lambda} d_{\lambda\lambda}^{\lambda q\lambda} D_{B=q}}{P_{\lambda}^h \sum_q q d_{++}^{\lambda q\lambda} d_{\lambda\lambda}^{\lambda q\lambda} D_{B=q}}; \quad (44)$$

while for unpolarized leptons but longitudinally polarized protons we have

$$P_{[\lambda;\lambda]}^{(0;\lambda)}(B) = \frac{P_{\lambda}^h \sum_q q (d_{++}^{\lambda q\lambda} + d_{+}^{\lambda q\lambda}) d_{\lambda\lambda}^{\lambda q\lambda} D_{B=q}}{P_{\lambda}^h \sum_q q (d_{++}^{\lambda q\lambda} + d_{+}^{\lambda q\lambda}) d_{\lambda\lambda}^{\lambda q\lambda} D_{B=q}}; \quad (45)$$

Finally, the most interesting case is when neither the proton nor the lepton are polarized: in this case the longitudinal polarization of baryon B is non-zero only due to parity violating weak contributions. We obtain

$$P_{[\lambda;\lambda]}^{(0;0)}(B) = \frac{P_{\lambda}^h \sum_q q d_{++}^{\lambda q\lambda} d_{+}^{\lambda q\lambda} d_{\lambda\lambda}^{\lambda q\lambda} D_{B=q}}{4 P_{\lambda}^h \sum_q q d_{\lambda\lambda}^{\lambda q\lambda} D_{B=q}}; \quad (46)$$

where $d^{\text{unpol}}_{\text{q}}$ is the unpolarized $\text{q}^+ \text{q}^-$ cross-section

$$4d^{\text{unpol}}_{\text{q}} = d^{\text{unpol}}_{++} + d^{\text{unpol}}_{+-} + d^{\text{unpol}}_{-+} + d^{\text{unpol}}_{--} ; \quad (47)$$

This effect might be measurable at HERA and numerical estimates will be given in the next Section.

5. Numerical estimates

In the previous Sections we have obtained explicit expressions for the polarization of baryons produced in DIS scatterings involving weak interactions; we now use these formulae to give predictions in the case of $\text{q}^+ \text{q}^-$ production, considering typical kinematical configurations of ongoing or planned experiments. When convenient, we integrate over the actual physical ranges of some variables; these are collected in Table 1 of Appendix A. Our results should give a good comprehensive description of what to expect in all present or future experiments, and can be adapted to cover all realistic situations, according to different kinematical cuts and configurations.

The polarization values depend on the known Standard Model dynamics, on the rather well known partonic distributions, both unpolarized and polarized, and on the quark fragmentation functions, again both unpolarized and polarized. The latter are not so well known and a choice must be made in order to give numerical estimates or in order to be able to interpret the measured values in favour of a particular set.

Unpolarized fragmentation functions are determined by fitting $e^+e^- \rightarrow \text{q}^+ \text{q}^- + X$ experimental data, which are sensitive only to singlet combinations, like $D_{=q} + D_{=q} = D_{(+)=q}$. It is impossible to separate the fragmentation functions relative to u 's from those for d 's in a model independent way; also flavour separation is not possible without appropriate initial assumptions, for example about SU(3) flavour symmetry. Polarized fragmentation functions are obtained by fitting the scarce data on $\text{q}^+ \text{q}^-$ polarization at LEP, sensitive only to non-singlet combinations like $D_{=q} - D_{=q} = D_{=q}^{\text{val}}$. Also in this case flavour separation has to rely on models.

Three typical sets of fragmentation functions, denoted as scenarios 1, 2 and 3, and derived from fits to e^+e^- data, are given in Ref. [4]. The unpolarized fragmentation functions are taken to be SU(3) symmetric:

$$D_{(+)=u} = D_{(+)=d} = D_{(+)=s} = D_{(+)=u} = D_{(+)=d} = D_{(+)=s} ; \quad (48)$$

and have been derived for the combined production of u and d and not for each of them separately.

For the polarized fragmentation functions they assume, at the initial scale Q_0^2 :

$$\begin{aligned} D_{=s}(z; Q_0^2) &= z D_{(+)=s}(z; Q_0^2) ; \\ D_{=u}(z; Q_0^2) &= D_{=d}(z; Q_0^2) = N_u D_{=s}(z; Q_0^2) ; \end{aligned} \quad (49)$$

The three scenarios differ for the relative contributions of the strange quark polarization to Δu polarization: $N_u = 0$, $N_u = 0.2$ and $N_u = 1$ for scenarios 1, 2 and 3 respectively [4]. The "unfavoured" polarized fragmentations $D_{s,u}^+$; $D_{s,u}^-$, etc. are assumed to be negligible at the initial scale Q_0^2 , and are only generated by QCD evolution; it is then possible, for the polarized fragmentation functions, to obtain separately the contributions to Δu and Δd .

We adopt the above set of fragmentation functions as they are the least dependent on models, they have the proper QCD evolution, and the three scenarios are well representative of possible spin dependences. We are then equipped with unpolarized fragmentation functions into $+$ and with separate polarized fragmentation functions into $+$ and $-$; we wish to give predictions and estimates for the polarizations of $+$ and $-$, which are measured separately. We then define the following computable quantities:

$$P^+(\Delta u) = \frac{d^+ + \Delta d^+}{d^+} = \frac{P^+(\Delta u)}{1 + T}; \quad (50)$$

and

$$P^-(\Delta u) = \frac{d^- + \Delta d^-}{d^-} = P^-(\Delta u) \frac{T}{1 + T}; \quad (51)$$

where the notations should be obvious and

$$T = \frac{d^+}{d^-} \quad (52)$$

Eqs. (50) and (51) allow to compute the values of $P^+(\Delta u)$ and $P^-(\Delta u)$ provided one can compute or measure the ratio T :

$$P^+(\Delta u) = (1 + T)P^-(\Delta u); \quad P^-(\Delta u) = \frac{1}{1 + T} P^+(\Delta u); \quad (53)$$

Notice that P^+ is always larger in magnitude than P^- .

The ratio T cannot be computed with the fragmentation set of Ref. [4]; it requires the knowledge of separate unpolarized fragmentation functions for $+$ and $-$ and it depends on the chosen set.

In Figs. 1-10 we show some results for $P^+(\Delta u)$ for several processes, with different initial spin configurations, and different kinematical conditions, corresponding to typical experimental setups, shown in Table 1 of Appendix A. These may easily be changed, according to experimental situations. Details are given in the figure captions. We use the unpolarized distribution functions of Refs. [14], the related polarized distribution functions of Ref. [15] (we have explicitly checked that our numerical results depend very little on the available sets of parton densities) and the fragmentation functions of Ref. [4], mainly with scenarios 2 and 3.

In Figs. 11-12 we give estimates for $P^-(\Delta u)$ [rather than $P^+(\Delta u)$], in the same cases of some of the previous figures; we have computed the ratio T either with the

SU (3) symmetric set of unpolarized fragmentation functions of Ref. [9] or with a set derived from Ref. [16], by imposing SU (3) symmetry.

The figure captions contain all relevant information about the various cases; we give here some general comments about our results.

We present results using mainly the fragmentation functions of scenarios 2 and 3 of Ref. [4], neglecting scenario 1, in which only s quarks contribute to polarization. In fact, $P_{[;]}^{(0)}$ is always negligible in this case, given the small content of s quarks in the nucleon target and the SU (3)-symmetric nature of the unpolarized fragmentation functions utilized. This can be seen by inspecting Eqs. (19), (20) and (26), (27) for charged current interactions and Eq. (37) for neutral currents. However, it is interesting to notice that for unpolarized fragmentation functions allowing for a strong SU (3) symmetry breaking, like those of Ref. [16], the situation can be different, and scenario 1 might give sizeable asymmetries. According to Ref. [16], $D_{=u} = D_{=d} = D_{=s}$ and this can well compensate for the small factor R in Eq. (20), so that, also in scenario 1, $P_{[;]}$ can be large.

Figs. 1, 2 and 11 summarize some of the most interesting features of polarization in charged current interactions. The large x_{1i} values involved in NOMAD experiment imply $T = d = d = 1$, so that, from Eq. (50), $P_{[;]}^{(0)}$ is similar to $P_{[;]}^{(1)}$ (compare Figs. 2 and 11) and follows closely the simple behaviour suggested by Eqs. (19) and (20). $P_{[;]}^{(0)}$, instead, is suppressed by the small ratio T , see Eq. (51); the actual estimated value of $P_{[;]}^{(0)}$ is shown in Fig. 11 and is much larger. Notice that a comparison between Figs. 1 and 2, i.e. between Eqs. (19) and (20), might give information on the ratios $C_q = D_{=q} = D_{=q}$; for example, the same value of C_q for all flavours would result in $P_{[;]}^{(0)} = P_{[;]}^{(1)}$. On the other hand, largely different values of $P_{[;]}^{(0)}$ and $P_{[;]}^{(1)}$ would certainly indicate a strong SU (3) symmetry breaking in the fragmentation functions, with s quark contributions dominating in order to compensate for the small R factor in Eq. (20).

Some data on $P_{[;]}^{(0)}(x;)$ are available from NOMAD collaboration [13], but the errors and uncertainties are still too large to allow significant comparisons and to discriminate between different sets of fragmentation functions.

Fig. 3 gives values of $P_{[;]}^{(0)}$ in kinematical regions dominated by small x values, so that one expects $T \approx 1$ and $P_{[;]}^{(0)}(x;)/P_{[;]}^{(1)}(x;) = 2$, Eqs. (50) and (51). The opposite signs of $P_{[;]}^{(0)}$ and $P_{[;]}^{(1)}$ can be easily understood by looking at Eq. (25) (with $q \neq q=2$) and noticing that fragmentation into a baryon or an antibaryon favours the first or the second term in the numerator.

For neutrino charged currents we give numerical estimates only in the case of an unpolarized target. In fact, present intensities of neutrino beams require very large targets to reach reasonable luminosities and statistics, and

this makes unpractical to polarize them. There are however proposals for neutrino factories with large intensities which will allow to consider the option of polarized targets [17].

The polarizations for neutral currents shown in Figs. 4, 5, 6 and 7 exhibit a similar behaviour for the four different kinematical setups considered. The differences are related to the different kinematical cuts and again to the value of the factor T . In particular, since $T \approx 1$ for E665 and HERA kinematics, the P are suppressed by a factor ≈ 2 with respect to the case of HERMES and COMPASS kinematics. Notice also that in these two cases there are sizeable variations depending on the different polarization states of the target.

The results presented in Figs. 8 and 12 show polarizations as functions of x (integrated over z) rather than z (integrated over x): these test the dynamics of the partonic process and in particular the contribution of electro-weak interferences, in a neat and unusual way. The differences between positively and negatively charged leptons are entirely due to electro-weak effects; this is well visible at large x (implying large Q^2), where the curves for e^+ and e^- differ sizeably. Moreover, from Eqs. (39)–(41) it is possible to evaluate analytically the zeros of the cross-section differences $d^+ + d^-$ appearing in the numerator of Eq. (44); one can show that real zeros for $0 < x < 1$ occur only for electromagnetic + weak contributions and for positron beams. The effective position of the zeros depends on y (or alternatively on Q^2) and for the dominating small y values is around $x \approx 0.04 - 0.08$. Although the statistical errors increase sizeably for large x values at HERA, the different behaviour shown at small and large x values for positron and electron beams might probably be tested.

Fig. 12 shows the same plots as in Fig. 8, for the actual polarization $P(\lambda)$, estimated according to the comments in the figure caption, rather than for $P(\lambda)$; it is interesting to note how the differences between P and P vary with x , according to the observations we have already made.

Fig. 9 shows the parity violating longitudinal polarization of γ 's produced from unpolarized initial electrons and nucleons in NC processes; being a purely electro-weak effect it is more sizeable at very large Q^2 values, which are, however, accessible at HERA. Also Fig. 10 shows some effects of electro-weak interferences, resulting in differences between plots of $P_{[e,\bar{e}]}^{(+,0)}$ for positrons and electrons.

We have given a comprehensive discussion { both theoretical (at LO) and phenomenological } of the polarization of γ 's and γ 's produced in the current fragmentation region of DIS processes, both with neutral and charged currents. Our results can be exploited to gather new information about polarized fragmentation functions, to improve our knowledge about polarized parton densities [18] and to test

fundamental features of electro-weak elementary interactions. Several experiments are either running or being planned, which will precisely look at these semi-inclusive DIS processes; our study should help in the analysis of the forthcoming data.

Acknowledgements

We would like to thank J.T. Londergan and A.W. Thomas for several discussions; M.A. is grateful to the Special Research Centre for the Subatomic Matter of Adelaide (Australia) for hospitality and support during a period in which this paper was in preparation. M.B. is most grateful for partial support from the EU-TMR Program, Contract No. CT98-0169 and wishes to thank the Dept. of Theoretical Physics of Torino University for hospitality and travel support. U.D. and F.M. thank COFINANZIAMENTO MURST-PRIN for partial support.

Appendix A { Experimental setups and kinem atical cuts

In our analysis we have considered most present and forthcoming experiments, which cover any different kinem atical configurations. For the reader's convenience, we collect and summarize here the corresponding experimental setups, with their kinem atical ranges.

The main variables which specify the various setups are listed below, while the kinem atical values and cuts for the different experiments are given in Table 1.

- E_l : incoming lepton energy, in the Laboratory reference frame
- \sqrt{s} : total energy, in the lepton-proton c.m. frame
- W : total energy, in the virtual boson-proton c.m. frame
- E_p : outgoing lepton energy, in the Laboratory frame
- $\theta_{(h)}$: outgoing lepton (hadron) scattering angle, in the Laboratory frame
- E_h : outgoing hadron energy, in the Laboratory frame
- p_T : transverse hadron momentum (w.r.t. the lepton direction)
- $\eta = \ln \tan(\theta_{(h)}=2)$, pseudorapidity, in the Laboratory frame

$x = Q^2=2q_p, y = q_p = \frac{p \cdot q}{p \cdot p} = \frac{p \cdot q}{p^2}$ are the usual invariant variables for semi-inclusive DIS hadron production.

	HERMES	COMPASS	E665	NOMAD	HERA	HERA*
E_l [GeV]	27.6	200	470	48.8	27.6	27.6
\sqrt{s} [GeV]	7.26	19.4	29.7	9.6	300	300
x	0.023-0.8	> 0.01	(10 ⁻³)-0.1	0.22	> 0.004	> 0.01
y	< 0.85	0.1-0.9	0.1-0.8	0.48	0.04-0.95	0.1-0.95
z	0.2-0.7	0.2-0.9	0.1-0.95		> 0.1	> 0.1
Q^2 [GeV ²]	1-24	> 4	(1)-2.5	9	10-2000	200-10 ⁴
W [GeV]	> 2			5.8		
E_p [GeV]	> 4.1		< 420		> 10	> 10
θ [rad]	0.04-0.22					
E_h [GeV]	> 2	> 5	> 4			
p_T [GeV]					> 0.5	{1.5-1.5}

Table 1: Summary of the experiments and the corresponding kinem atical setups.

Whenever possible we have considered kinematical cuts identical to those already adopted or planned for the related experiments; the Q^2 range for the E665 experiment at SLAC ($0.25 < Q^2 < 2.5 \text{ GeV}^2$) reaches too low Q^2 values for our leading order analysis, based on factorization theorem, and we have adopted the range $1.0 < Q^2 < 2.5 \text{ GeV}^2$ (this influences also the lower cut on x , of course).

Notice also that with HERA we mean both H1 and ZEUS typical setups at intermediate Q^2 values, while with HERA* we refer to setups with very high Q^2 values, as required for the study of electro-weak interference effects.

For NOMAD experiment, all kinematical variables are fixed to the corresponding average value [19].

Appendix B { Mass correction effects

In this paper fragmentation functions are always expressed as a function of $z = p_h / p_q$, where p_h, p_q are the four-momenta of the target proton, the produced hadron, and the virtual boson respectively. In the case of semi-inclusive DIS, at LO and in collinear configuration, z coincides with the light-cone momentum fraction of the parent parton carried by the observed hadron, $z = p_h^+ / p_q^+$. There are in general several other variables that can be considered; depending on the specific process under study, they can be more or less suitable than z to, e.g., describe the process from the experimental point of view or to show scaling properties of observables, like cross-sections. In this Appendix, we shortly review the definition of these variables and give the connection among them. It is important to notice that at very large energy scales E , when the mass of the observed hadron M_h can be safely neglected, all these variables coincide (excluding the regions where they are comparable to $M_h = E$). However, kinematics for most of the running or forthcoming experiments on semi-inclusive hadron production, which is the main subject of this paper, are such that mass corrections can be relevant. We always neglect corrections due to the mass of the proton target, even though they might have some effects in particular kinematical ranges.

Let us first briefly summarize the situation in the case of $e^+e^- \rightarrow X$ process, which is used to fix the set of fragmentation functions largely adopted in this paper. The variables usually utilized are:

$$\begin{aligned}
 x_E &= \frac{2p_h \cdot q}{Q^2} \equiv \frac{2E_h}{P^+}; \\
 x_p &= \frac{2|\mathbf{p}_h \cdot \mathbf{j}|}{Q} = \frac{2|\mathbf{p}_h \cdot \mathbf{j}|}{P^+}; \\
 &= \frac{p_h^+}{p_q^+};
 \end{aligned} \tag{54}$$

where p_h is the hadron three-momentum in the e^+e^- c.m. reference frame. x_E and x_p are usually adopted by the experimentalists, while z is more commonly used by the theorists. At large energies, like in e^+e^- collisions at the Z_0 pole, and considering

$x_E > 0.1$, which is also required for other theoretical reasons, see Ref. [4], mass effects are in fact negligible and all these variables can be safely assumed to be equivalent; the fragmentation function dependence on x_E can then be directly identified with the x_E dependence shown by the experimental results. When mass corrections are relevant, the connection among the variables defined in Eqs. (54) is given, at leading order, as follows:

$$\begin{aligned} x_p &= x_E ; \\ &= x_E \frac{1 + \sqrt{1 - 4x_E}}{2} ; \end{aligned} \quad (55)$$

where the factor $\sqrt{1 - 4x_E}$ is defined as

$$\sqrt{1 - 4x_E} = 1 - \frac{4M_h^2}{x_E^2 s} \quad (56)$$

Let us now consider the case of semi-inclusive DIS, in the virtual boson-target proton center of mass reference frame, for hadron production in the current fragmentation region ($x_F > 0$). Usual variables are:

$$\begin{aligned} z &= \frac{p \cdot p_h}{p \cdot q} = \frac{E_h + |\vec{p}_h|}{W} ; \\ x_F &= \frac{2p_L}{W} = \frac{2|\vec{p}_h|}{W} ; \\ z^0 &= \frac{E_h}{E_{q^0}} = \frac{E_h}{(1 - x)E_p} = \frac{2E_h}{W} ; \end{aligned} \quad (57)$$

where E_{q^0} is the energy of the parent quark in the process $q^0 \rightarrow h + X$. x_F and z are the variables usually adopted by the experimentalists. However, as shown in Ref. [4], the appropriate scaling variable for semi-inclusive DIS is z^0 rather than x_F .

Defining $M_h = W$, the ranges of variation of the three variables are

$$\begin{aligned} x_F &\in [0; 1 - 4^{2-1=2}] ; \\ z^0 &\in [2^{-1} \frac{M_h}{2} ; 1] ; \\ z &\in [2^{-1} \frac{1}{2} ; 1 + \frac{1}{2} 4^{2-1=2}] : \end{aligned} \quad (58)$$

The expressions of the three variables as a function of the other two are

$$x_F = z^0 \frac{1 + \sqrt{1 - 4z^0}}{2} ; \quad x_F = z \frac{1 + \sqrt{1 - 4z}}{2} ; \quad (59)$$

$$z^0 = x_F \frac{1 + \sqrt{1 - 4x_F}}{2} ; \quad z^0 = z \frac{1 + \sqrt{1 - 4z}}{2} ; \quad (60)$$

$$z = x_F \frac{1}{2} \left(1 + \sqrt{1 + 4 \frac{1 - x_F^2}{x_F^2}} \right) ; \quad z = z^0 \frac{1}{2} \left(1 + \sqrt{1 + 4 \frac{1 - z^0^2}{z^0^2}} \right) ; \quad (61)$$

If we start from, e.g., a cross-section evaluated in our formalism (we omit here the dependence on x and y)

$$\frac{d}{dz} / D_h(z); \quad (62)$$

the corresponding cross-section expressed as a function of x_F will be given by

$$\frac{d}{dx_F} = \frac{dz}{dx_F} \frac{d}{dz} / D_h[z(x_F)]; \quad (63)$$

where, apart from the overall rescaling factor $dz=dx_F$, one must keep into account that fragmentation functions, obtained in the variable z , are to be rescaled to the z value corresponding to x_F .

In variables like polarizations, given as ratios of two cross-sections, the overall rescaling factors cancel out and the remaining effect is the rescaling between the two variables in the fragmentation functions, according to Eqs. (59)–(61).

Of course, if the average value of the polarization over a given kinematical region is required, the appropriate overall rescaling factors, like $dz=dx_F$ in Eq. (63), have to be taken into account in the kinematical integrations.

References

- [1] M. Anselmino, M. Boglione, J. Hansson and F. Murgia, *Phys. Rev. D* 54 (1996) 828
- [2] R. L. Jaffe, *Phys. Rev. D* 54 (1996) 6581
- [3] J. Ellis, D. Kharzeev and A. Kotzinian, *Z. Phys. C* 69 (1996) 467
- [4] D. de Florian, M. Stratmann and W. Vogelsang, *Phys. Rev. D* 57 (1998) 5811
- [5] A. Kotzinian, A. Bravar and D. von Harrach, *Eur. Phys. J. C* 2 (1998) 329
- [6] A. Kotzinian, talk at the VII Workshop on High Energy Spin Physics (SPIN-97), 7-12 July 1997, Dubna, Russia; e-Print Archive: hep-ph/9709259
- [7] S.L. Bebestotski, *Nucl. Phys. B* 79 (Proc. Suppl.) (1999) 526
- [8] D. Boer, R. Jakob and P.J. Mulders, *Nucl. Phys. B* 564 (2000) 471
- [9] C. Boros, J.T. Londergan and A.W. Thomas, *Phys. Rev. D* 61 (2000) 014007
- [10] D. Ashery and H.J. Lipkin, *Phys. Lett. B* 469 (1999) 263
- [11] B-Q. Ma, I. Schmidt, J. Soer and J-Y. Yang, *Eur. Phys. J. C* 16 (2000) 657; *Phys. Rev. D* 62 (2000) 114009
- [12] M. Anselmino, M. Boglione and F. Murgia, *Phys. Lett. B* 481 (2000) 253
- [13] NOMAD Collaboration, P. Aster et al., *Nucl. Phys. B* 588 (2000) 3; e-Print Archive: hep-ex/0103047
- [14] M. Glück, E. Reya and A. Vogt, *Z. Phys. C* 67 (1995) 433
- [15] M. Glück, E. Reya, M. Stratmann and W. Vogelsang, *Phys. Rev. D* 53 (1996) 4775
- [16] D. Indumathi, H.S. Mani and A. Rastogi, *Phys. Rev. D* 58 (1998) 094014
- [17] M.L. Mangano et al., CERN report CERN-TH/2001-131, e-Print Archive: hep-ex/0105155
- [18] M. Anselmino, M. Boglione, U.D'Alesio, E. Leader and F. Murgia, *Phys. Lett. B* 509 (2001) 246
- [19] D.V. Naumov, private communication

Figure captions

Fig. 1: $P_{[;]}^{(0)}$ for (solid lines) and (dashed lines) hyperons, as a function of z , with a kinematical setup typical of NOMAD experiment at CERN (see Table 1 for details). Results are given for scenarios 2 and 3 of the polarized FF of Ref. [4]. Results with scenario 1 are almost negligible. Unpolarized (+) FF are from Ref. [4]; unpolarized GRV [14] partonic distributions have been used for the proton target. Since hx_i is large for this kinematical configuration, we expect $T = d = d = 1$ and, as a consequence, $P_{[;]}^{(0)}(\cdot) \approx P_{[;]}^{(0)}(\cdot)$, while $P_{[;]}^{(0)}(\cdot) \approx P_{[;]}^{(0)}(\cdot)$ (see text for more details).

Fig. 2: $P_{[;]}^{(0)}$ for (solid lines) and (dashed lines) hyperons, as a function of z , with a kinematical setup typical of NOMAD experiment at CERN (see Table 1 for details). Results are given for scenarios 2 and 3 of the polarized FF of Ref. [4]. Results with scenario 1 are almost negligible. Unpolarized (+) FF are from Ref. [4]; unpolarized GRV [14] partonic distributions have been used for the proton target. Since hx_i is large for this kinematical configuration, we expect $T = d = d = 1$ and, as a consequence, $P_{[;]}^{(0)}(\cdot) \approx P_{[;]}^{(0)}(\cdot)$, while $P_{[;]}^{(0)}(\cdot) \approx P_{[;]}^{(0)}(\cdot)$ (see text and Fig. 11 for more details).

Fig. 3: $P_{[e;]}^{(0)}$ for (solid lines) and (dashed lines) hyperons, as a function of z , with a kinematical setup typical of HERA experiments at DESY (see Table 1 for details). Results are given for scenarios 2 and 3 of the polarized FF of Ref. [4]. Results with scenario 1 are almost negligible. Unpolarized (+) FF are from Ref. [4]; unpolarized GRV [14] partonic distributions have been used for the proton target. Since hx_i is small for HERA kinematical configurations, we expect $T = d = d \neq 1$ and, as a consequence, $P_{[e;]}^{(0)}(\cdot) \approx 2P_{[e;]}^{(0)}(\cdot)$ (see text for more details).

Fig. 4: $P_{[e;e]}^{(0)}$ for hyperons, as a function of z , for different combinations of the beam and target polarizations, as shown in the plot legend. The kinematical setup is typical of HERMES experiment at DESY (see Table 1 for details). Results are given for scenarios 2 (heavy lines) and 3 (thin lines) of the polarized FF of Ref. [4]. Results with scenario 1 are almost negligible. Unpolarized (+) FF are from Ref. [4]; unpolarized GRV [14] and polarized GRSV-ST [15] partonic distributions have been used for the proton target. Since hx_i is large for HERMES kinematical configuration, we expect, at large z , $T = d = d = 1$ and, as a consequence, $P_{[e;e]}^{(0)}(\cdot) \approx P_{[e;e]}^{(0)}(\cdot)$, while for the (not shown in this plot) it should result $P_{[e;e]}^{(0)}(\cdot) \approx P_{[e;e]}^{(0)}(\cdot)$ (see text for more details).

Fig. 5: $P_{[;]}^{(0)}$ for hyperons, as a function of z , for different combinations of the beam and target polarizations, as shown in the plot legend. The kinematical setup is typical of COMPASS experiment at CERN (see Table 1 for details). Results

are given for scenarios 2 (heavy lines) and 3 (thin lines) of the polarized FF of Ref. [4]. Results with scenario 1 are almost negligible. Unpolarized (+) FF are from Ref. [4]; unpolarized GRV [14] and polarized GRSV-ST [15] partonic distributions have been used for the proton target. Since hx_i is relatively large for COMPASS kinematical configuration, we expect, at large z , $T = d = d' = 1$ and, as a consequence, $P_{[;]}(\cdot) \approx P_{[;]}(\cdot)$, while for the (not shown in this plot) it should result $P_{[;]}(\cdot) \approx 2P_{[;]}(\cdot)$ (see text for more details).

Fig. 6: $P_{[;]}$ for hyperons, as a function of z , for different combinations of the beam and target polarizations, as shown in the plot legend. The kinematical setup is typical of E665 experiment at SLAC (see Table 1 for details). Results are given for scenarios 2 (heavy lines) and 3 (thin lines) of the polarized FF of Ref. [4]. Results with scenario 1 are almost negligible. Unpolarized (+) FF are from Ref. [4]; unpolarized GRV [14] and polarized GRSV-ST [15] partonic distributions have been used for the proton target. Since hx_i is relatively small for E665 kinematical configuration, we expect $T = d = d' \neq 1$ and, as a consequence, $P_{[;]}(\cdot) \approx 2P_{[;]}(\cdot)$ (see text for more details).

Fig. 7: $P_{[e;e]}$ for hyperons, as a function of z , for different combinations of the positron beam and target polarizations, as shown in the plot legend. The kinematical setup is typical of HERA experiments at DESY (see Table 1 for details). Results are given for scenarios 2 (heavy lines) and 3 (thin lines) of the polarized FF of Ref. [4]. Results with scenario 1 are almost negligible. Unpolarized (+) FF are also from Ref. [4]; unpolarized GRV [14] and polarized GRSV-ST [15] partonic distributions have been used for the proton target. Since hx_i is small for HERA kinematical configurations, we expect $T = d = d' \neq 1$ and, as a consequence, $P_{[e;e]}(\cdot) \approx 2P_{[e;e]}(\cdot)$ (see text for more details).

Fig. 8: $P_{[e;e]}^{(+;0)}$ for hyperons, as a function of x , both for positron (heavy lines) and electron (thin lines) beams. The kinematical setup is typical of HERA experiments at DESY (see Table 1 for details). Results are given for all the three scenarios of the polarized FF of Ref. [4]. Unpolarized (+) FF are from Ref. [4]; unpolarized GRV [14] partonic distributions have been used for the proton target. The crossing at $x \approx 0.1$ for the case of positron beam is due to the interference between electromagnetic and weak contributions. Since $T = d = d'$ is $\neq 1$ at large x and becomes comparable to unity at very low x , we expect, correspondingly, $P_{[e;e]}(\cdot) \approx P_{[e;e]}(\cdot)$ and $P_{[e;e]}(\cdot) \approx 2P_{[e;e]}(\cdot)$ (see text and Fig. 12 for more details).

Fig. 9: $P_{[e;e]}^{(0;0)}$ for hyperons, as a function of z , for various "high- Q^2 " options of the HERA kinematical setup (see the HERA* setup in Table 1 for details) and for a positron beam: $y > 0.1$ (solid lines); $y > 0.6$ (dashed lines); $Q^2 > 4000 \text{ GeV}^2$ (dot-dashed lines). Results are given for scenarios 2 (heavy lines) and 3 (thin lines) of the polarized FF of Ref. [4]. Results with scenario 1 are almost negligible. Unpolarized

(+) FF are from Ref. [4]; unpolarized GRV [14] partonic distributions have been used for the proton target (see text for more details).

Fig. 10: $P_{[e;e]}^{(+;0)}$ for hyperons, as a function of z , both for positron (heavy lines) and electron (thin lines) beams, and for various "high- Q^2 " options of the HERA kinematical setup (see the HERA * setup in Table 1 for details): $y > 0.1$ (solid lines); $y > 0.6$ (dashed lines). Results are given for scenarios 2 and 3 of the polarized FF of Ref. [4]. Results with scenario 1 are almost negligible. Unpolarized (+) FF are from Ref. [4]; unpolarized GRV [14] partonic distributions have been used for the proton target (see text for more details).

Fig. 11: $P_{[;]}^{(0)}$ for (solid lines) and (dashed lines) hyperons, as a function of z , with a kinematical setup typical of NOMAD experiment at CERN (see Table 1 for details). Results are given for scenarios 2 and 3 of the polarized FF of Ref. [4]. Results with scenario 1 are almost negligible. Unpolarized (+) FF are from Ref. [4]; unpolarized GRV [14] partonic distributions have been used for the proton target. Estimates for $P_{[;]}^{(0)}$ are obtained from Eqs. (53) by using the corresponding results for $P_{[;]}^{(0)}$, shown in Fig. 2, and evaluating $T = d = d$ with the , unpolarized FF of Ref. [9] (heavy lines) and Ref. [16] (thin lines); this last set has been modified by imposing SU(3) symmetry. The spread between the two corresponding sets of curves gives a good indication of the uncertainty due to the evaluation of the ratio T . Notice that this uncertainty is almost negligible for large z , where polarizations are expected to be sizeable for both scenarios 2 and 3.

Fig. 12: $P_{[e;e]}^{(+;0)}$ for hyperons, as a function of x , both for positron (heavy lines) and electron (thin lines) beams. The kinematical setup is typical of HERA experiments at DESY (see Table 1 for details). Results are given for all the three scenarios of the polarized FF of Ref. [4]. Unpolarized (+) FF are from Ref. [4]; unpolarized GRV [14] partonic distributions have been used for the proton target. Estimates for $P_{[e;e]}^{(+;0)}$ are obtained from Eqs. (53) by using the corresponding results for $P_{[e;e]}^{(+;0)}$, shown in Fig. 8, and evaluating $T = d = d$ with the unpolarized FF of Ref. [9]. The crossing at $x \approx 0.1$ for the case of positron beam is due to the interference between electromagnetic and weak contributions. Since $T = d = d$ is 1 at large x and becomes comparable to unity at very low x , we find, correspondingly, $P_{[e;e]}(\) \approx P_{[e;e]}(\)$ and $P_{[e;e]}(\ ;) \approx 2P_{[e;e]}(\ ;)$ (see text and Fig. 8 for more details).

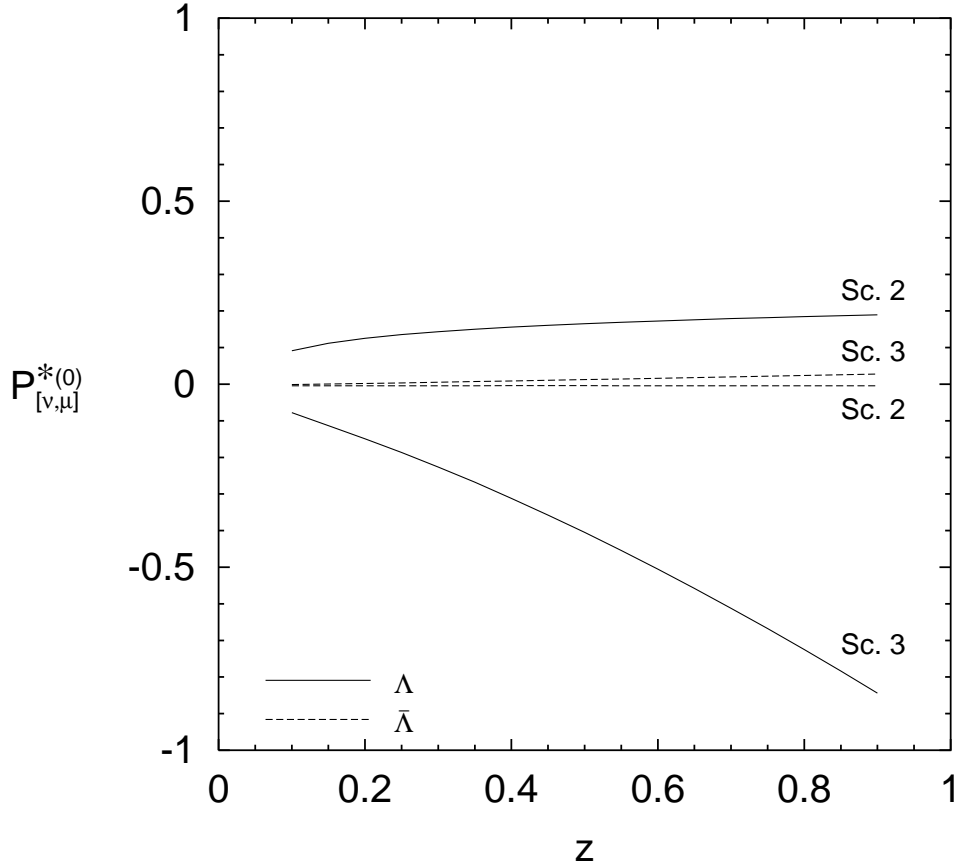


Figure 1: $P_{[;]}^{(0)}$ for Λ (solid lines) and $\bar{\Lambda}$ (dashed lines) hyperons, as a function of z , with a kinematical setup typical of NOMAD experiment at CERN (see Table 1 for details). Results are given for scenarios 2 and 3 of the polarized fragmentation functions (FF) of Ref. [4]. Results with scenario 1 are almost negligible. Unpolarized (+) FF are from Ref. [4]; unpolarized GRV [14] partonic distributions have been used for the proton target. Since x_{1i} is large for this kinematical configuration, we expect $T = d = \bar{d} = 1$ and, as a consequence, $P_{[;]}^{(0)}(\Lambda) \approx P_{[;]}^{(0)}(\bar{\Lambda})$, while $P_{[;]}^{(0)}(\Lambda) \approx -P_{[;]}^{(0)}(\bar{\Lambda})$ (see text for more details).

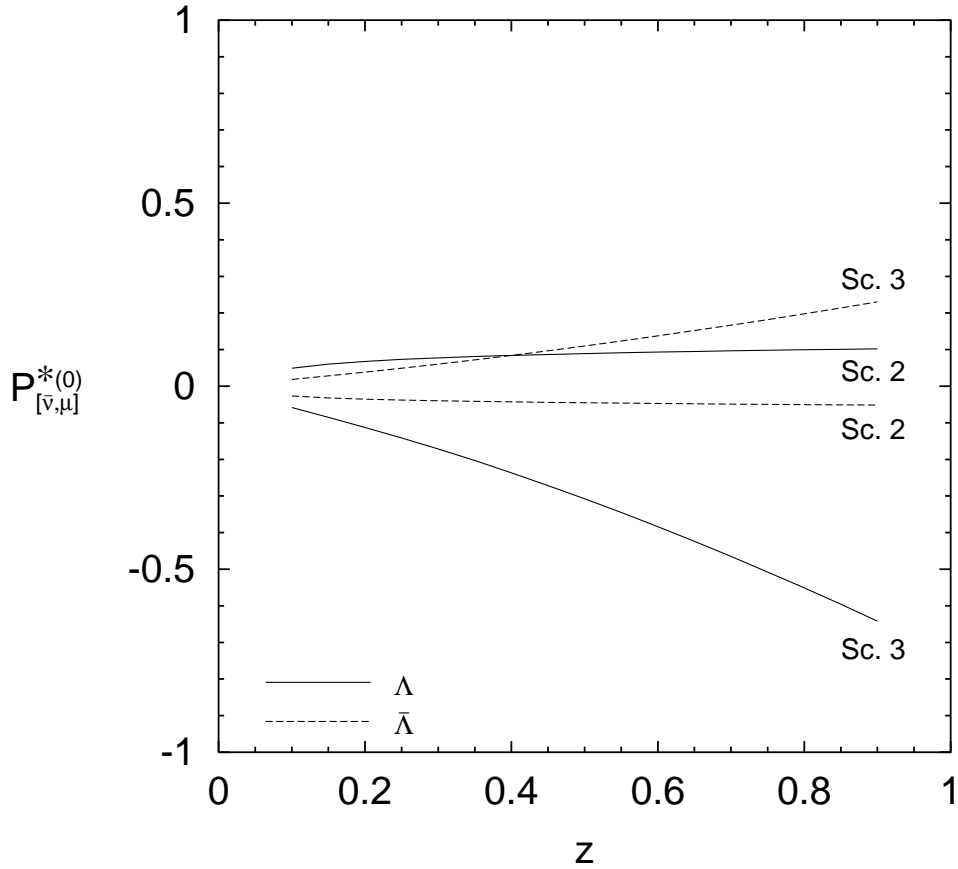


Figure 2: $P_{[v;\mu]}^{*(0)}$ for Λ (solid lines) and $\bar{\Lambda}$ (dashed lines) hyperons, as a function of z , with a kinematical setup typical of NOMAD experiment at CERN (see Table 1 for details). Results are given for scenarios 2 and 3 of the polarized FF of Ref. [4]. Results with scenario 1 are almost negligible. Unpolarized (+) FF are from Ref. [4]; unpolarized GRV [14] partonic distributions have been used for the proton target. Since hx_i is large for this kinematical configuration, we expect $T = d = \bar{d} = 1$ and, as a consequence, $P_{[v;\mu]}^{(0)}(\Lambda) \neq P_{[v;\mu]}^{(0)}(\bar{\Lambda})$, while $P_{[v;\mu]}^{(0)}(\Lambda) = P_{[v;\mu]}^{(0)}(\bar{\Lambda})$ (see text and Fig. 11 for more details).

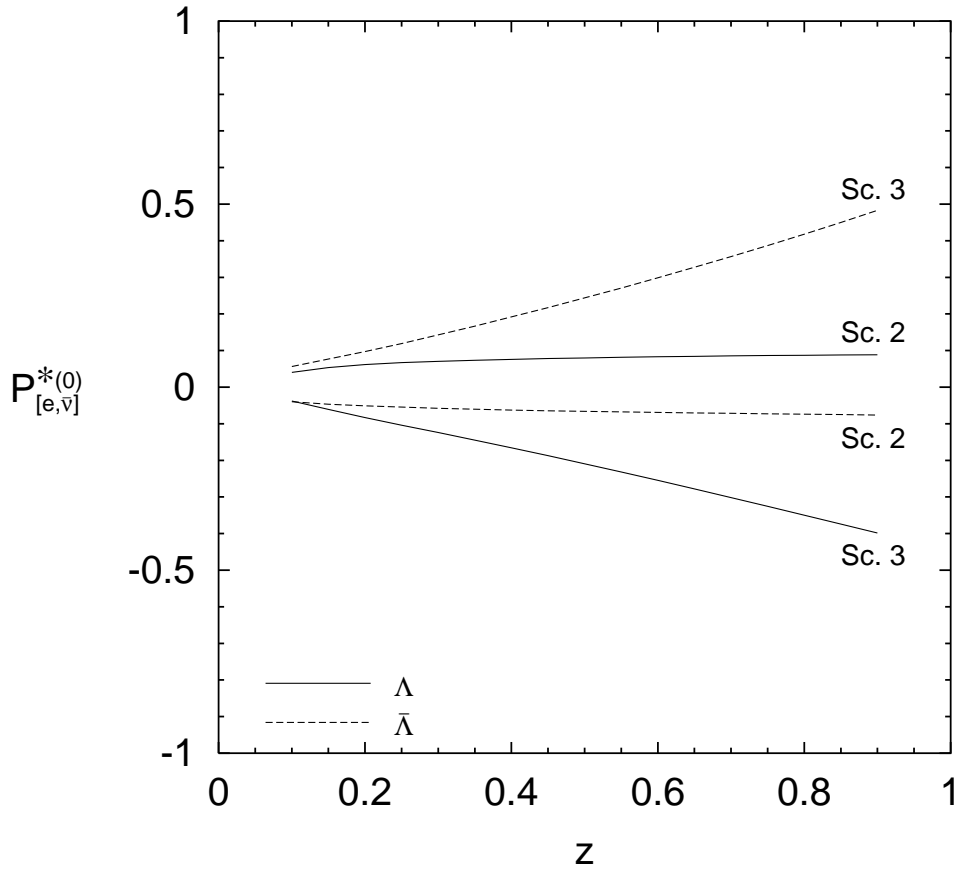


Figure 3: $P_{[e,v]}^{*(0)}$ for Λ (solid lines) and $\bar{\Lambda}$ (dashed lines) hyperons, as a function of z , with a kinematical setup typical of HERA experiments at DESY (see Table 1 for details). Results are given for scenarios 2 and 3 of the polarized FF of Ref. [4]. Results with scenario 1 are almost negligible. Unpolarized (+) FF are from Ref. [4]; unpolarized GRV [14] partonic distributions have been used for the proton target. Since h_{xi} is small for HERA kinematical configurations, we expect $T = d = d' = 1$ and, as a consequence, $P_{[e,v]}^{*(0)}(\xi) \approx 2P_{[e,v]}^{(0)}(\xi)$ (see text for more details).

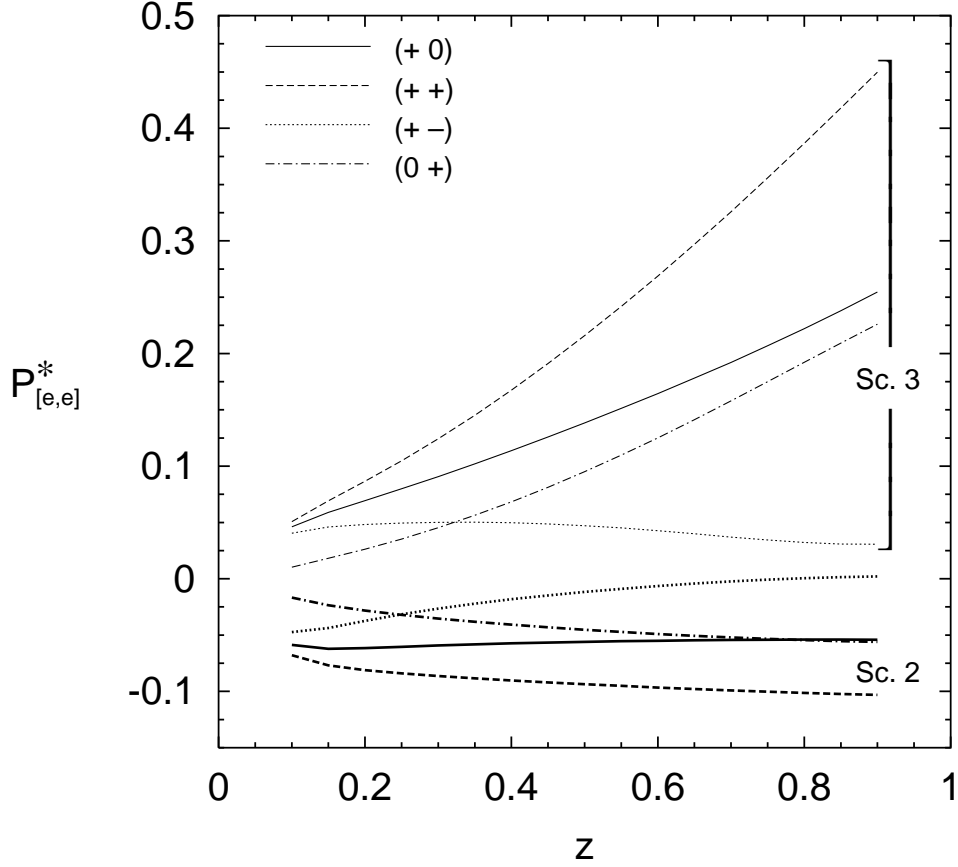


Figure 4: $P_{[e,e]}^*$ for hyperons, as a function of z , for different combinations of the beam and target polarizations, as shown in the plot legend. The kinematical setup is typical of HERMES experiment at DESY (see Table 1 for details). Results are given for scenarios 2 (heavy lines) and 3 (thin lines) of the polarized FF of Ref. [4]. Results with scenario 1 are almost negligible. Unpolarized ($+$) FF are from Ref. [4]; unpolarized GRV [14] and polarized GRSV-ST [15] partonic distributions have been used for the proton target. Since x_1 is large for HERMES kinematical configuration, we expect, at large z , $T = d = d = 1$ and, as a consequence, $P_{[e,e]}^*(z) \approx P_{[e,e]}(z)$, while for the (not shown in this plot) it should result $P_{[e,e]}^*(z) \approx P_{[e,e]}(z)$ (see text for more details).

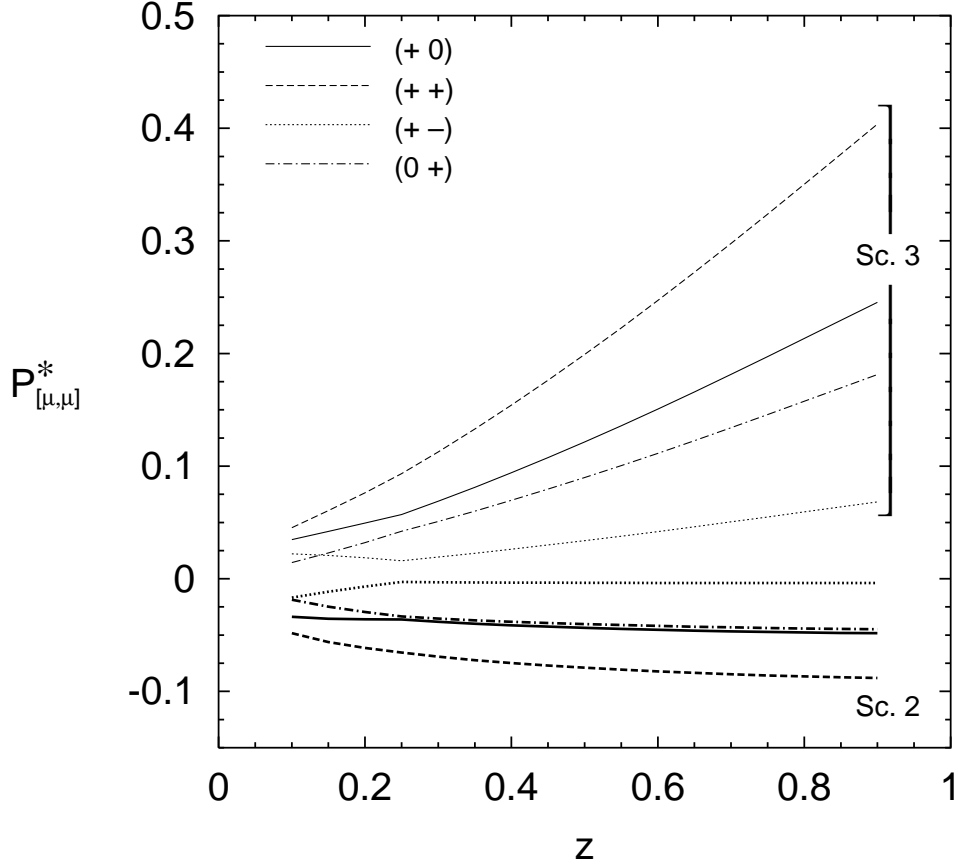


Figure 5: $P_{[;]}^*$ for hyperons, as a function of z , for different combinations of the beam and target polarizations, as shown in the plot legend. The kinematical setup is typical of COMPASS experiment at CERN (see Table 1 for details). Results are given for scenarios 2 (heavy lines) and 3 (thin lines) of the polarized FF of Ref. [4]. Results with scenario 1 are almost negligible. Unpolarized ($+$) FF are from Ref. [4]; unpolarized GRV [14] and polarized GRSV-ST [15] partonic distributions have been used for the proton target. Since hx_i is relatively large for COMPASS kinematical configuration, we expect, at large z , $T = d = d = 1$ and, as a consequence, $P_{[;]}^*(z) \approx P_{[;]}(z)$, while for the (not shown in this plot) it should result $P_{[;]}^*(z) \approx P_{[;]}(z)$ (see text for more details).

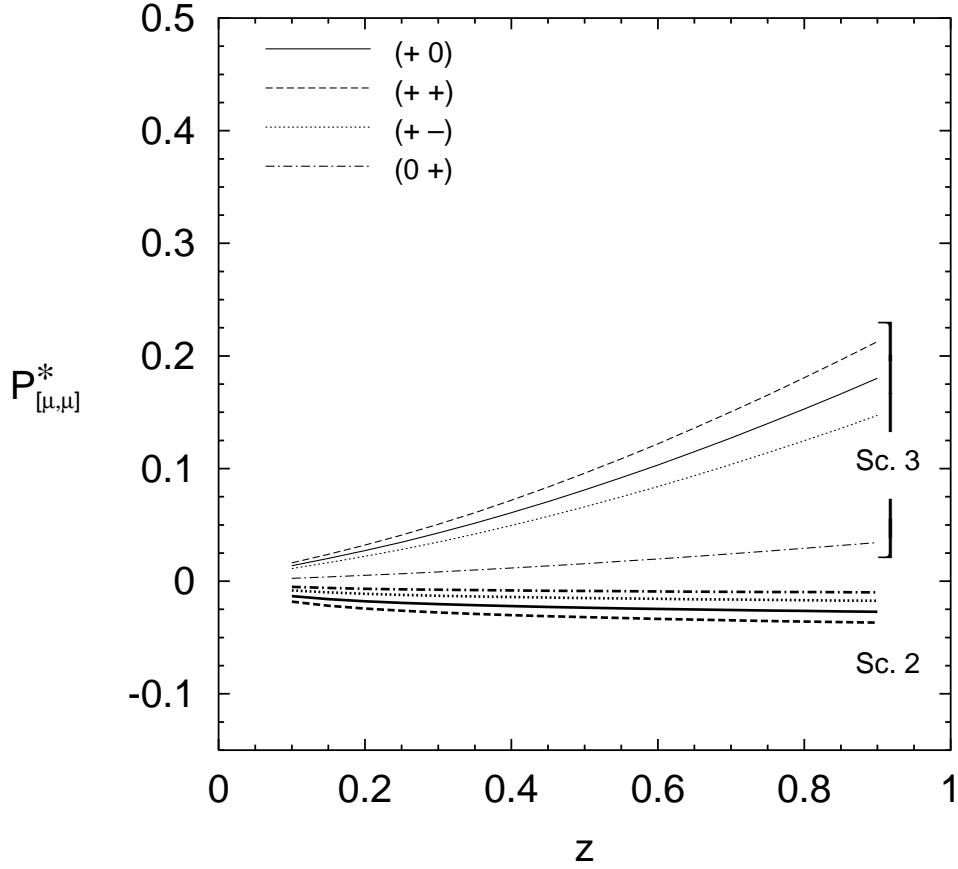


Figure 6: $P_{[\mu,\mu]}^*$ for hyperons, as a function of z , for different combinations of the beam and target polarizations, as shown in the plot legend. The kinematical setup is typical of E665 experiment at SLAC (see Table 1 for details). Results are given for scenarios 2 (heavy lines) and 3 (thin lines) of the polarized FF of Ref. [4]. Results with scenario 1 are almost negligible. Unpolarized ($++$) FF are from Ref. [4]; unpolarized GRV [14] and polarized GRSV-ST [15] partonic distributions have been used for the proton target. Since x_1 is relatively small for E665 kinematical configuration, we expect $T = d = d' = 1$ and, as a consequence, $P_{[\mu,\mu]}^*(+;+) = 2P_{[\mu,\mu]}^*(+0)$ (see text for more details).

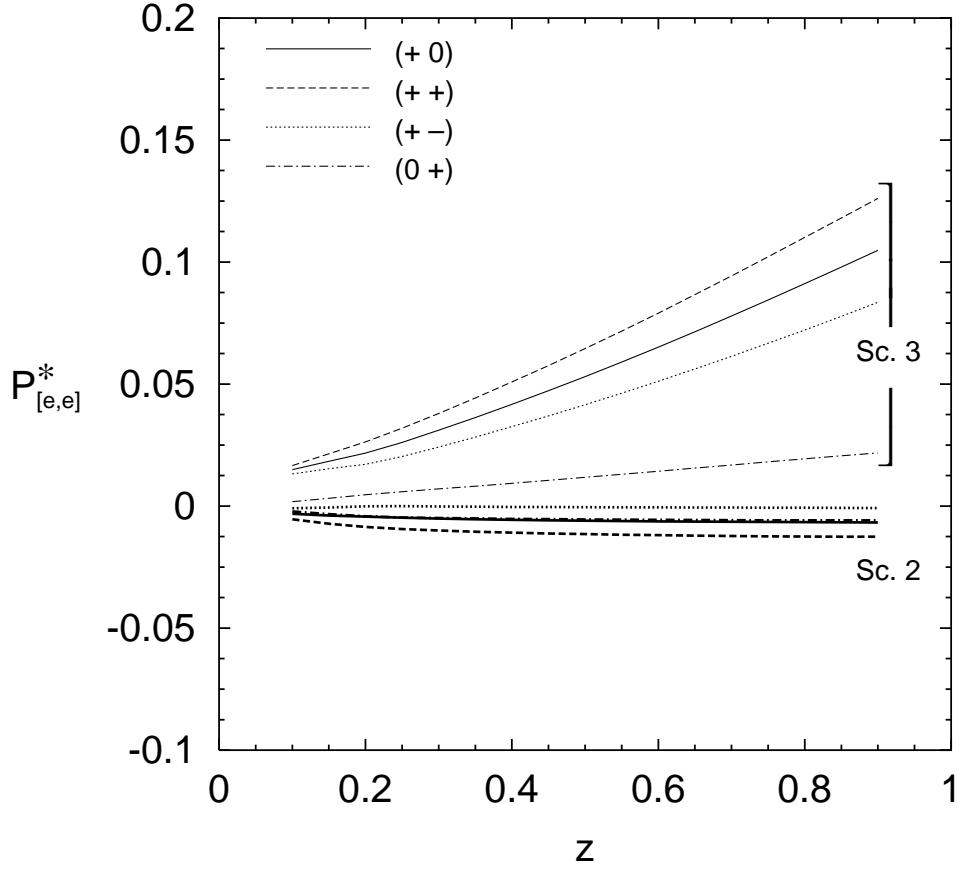


Figure 7: $P_{[e,e]}^*$ for hyperons, as a function of z , for different combinations of the positron beam and target polarizations, as shown in the plot legend. The kinematical setup is typical of HERA experiments at DESY (see Table 1 for details). Results are given for scenarios 2 (heavy lines) and 3 (thin lines) of the polarized FF of Ref. [4]. Results with scenario 1 are almost negligible. Unpolarized $(+)$ FF are also from Ref. [4]; unpolarized GRV [14] and polarized GRSV-ST [15] partonic distributions have been used for the proton target. Since $\langle x_i \rangle$ is small for HERA kinematical configurations, we expect $T = d = d' = 1$ and, as a consequence, $P_{[e,e]}^*(;)' = 2P_{[e,e]}(;)$ (see text for more details).

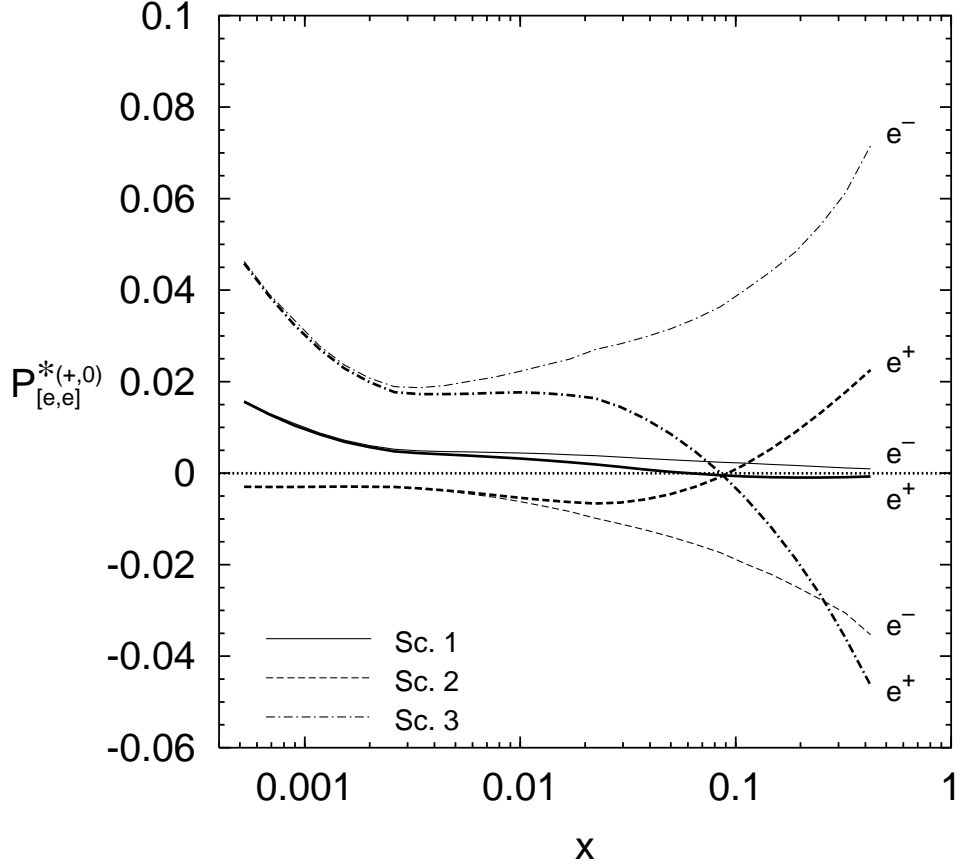


Figure 8: $P_{[e,e]}^{*(+,0)}$ for hyperons, as a function of x , both for positron (heavy lines) and electron (thin lines) beams. The kinematical setup is typical of HERA experiments at DESY (see Table 1 for details). Results are given for all the three scenarios of the polarized FF of Ref. [4]. Unpolarized (+) FF are from Ref. [4]; unpolarized GRV [14] partonic distributions have been used for the proton target. The crossing at $x \approx 0.1$ for the case of positron beam is due to the interference between electromagnetic and weak contributions. Since $T = d = \bar{d}$ is 1 at large x and becomes comparable to unity at very low x , we expect, correspondingly, $P_{[e,e]}^{*(+,0)} \approx P_{[e,e]}^{*(-,0)}$ and $P_{[e,e]}^{*(+,0)} \approx 2P_{[e,e]}^{*(-,0)}$ (see text and Fig. 12 for more details).

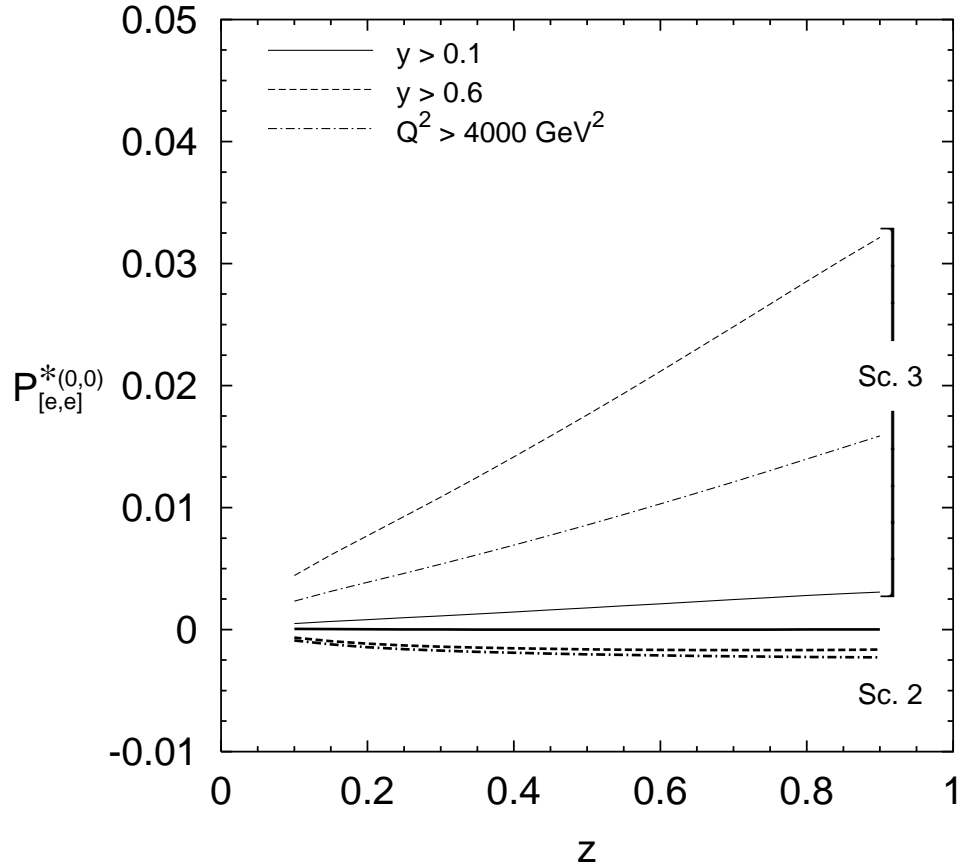


Figure 9: $P_{[e,e]}^{*(0,0)}$ for hyperons, as a function of z , for various "high- Q^2 " options of the HERA kinematical setup (see the HERA * setup in Table 1 for details) and for a positron beam : $y > 0.1$ (solid lines); $y > 0.6$ (dashed lines); $Q^2 > 4000 \text{ GeV}^2$ (dot-dashed lines). Results are given for scenarios 2 (heavy lines) and 3 (thin lines) of the polarized FF of Ref. [4]. Results with scenario 1 are almost negligible. Unpolarized (+) FF are from Ref. [4]; unpolarized GRV [14] partonic distributions have been used for the proton target (see text for more details).

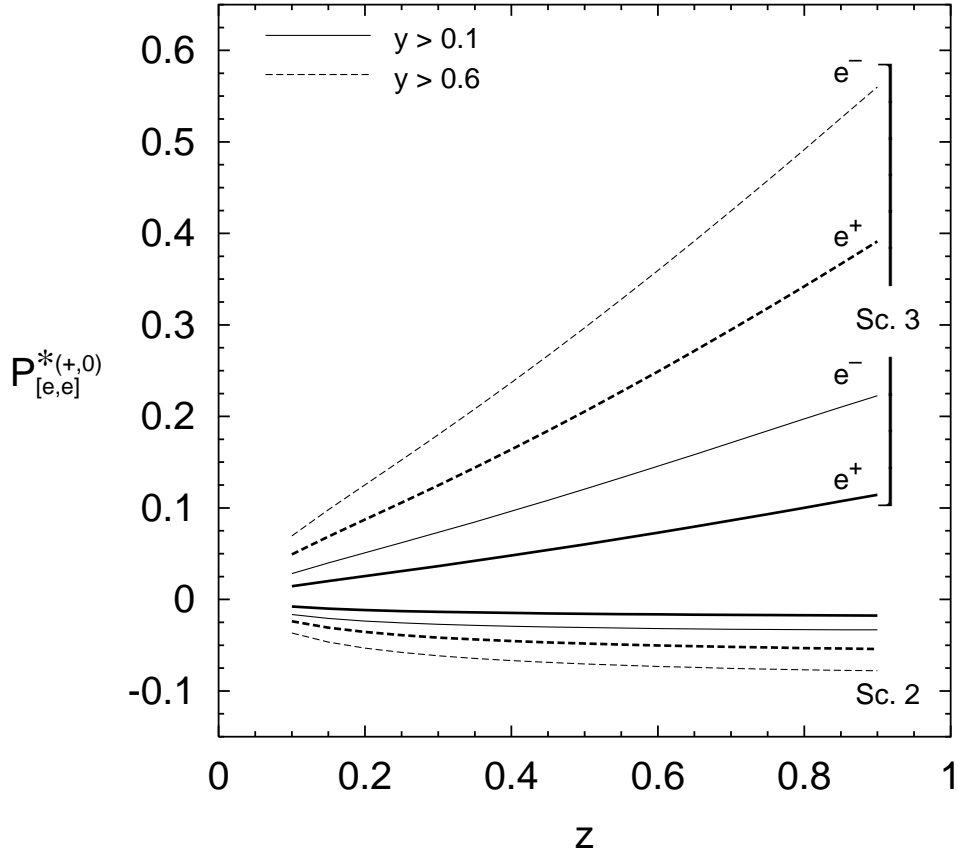


Figure 10: $P_{[e,e]}^{*(+,0)}$ for hyperons, as a function of z , both for positron (heavy lines) and electron (thin lines) beams, and for various "high- Q^2 " options of the HERA kinematical setup (see the HERA* setup in Table 1 for details): $y > 0.1$ (solid lines); $y > 0.6$ (dashed lines). Results are given for scenarios 2 and 3 of the polarized FF of Ref. [4]. Results with scenario 1 are almost negligible. Unpolarized (+) FF are from Ref. [4]; unpolarized GRV [14] partonic distributions have been used for the proton target (see text for more details).

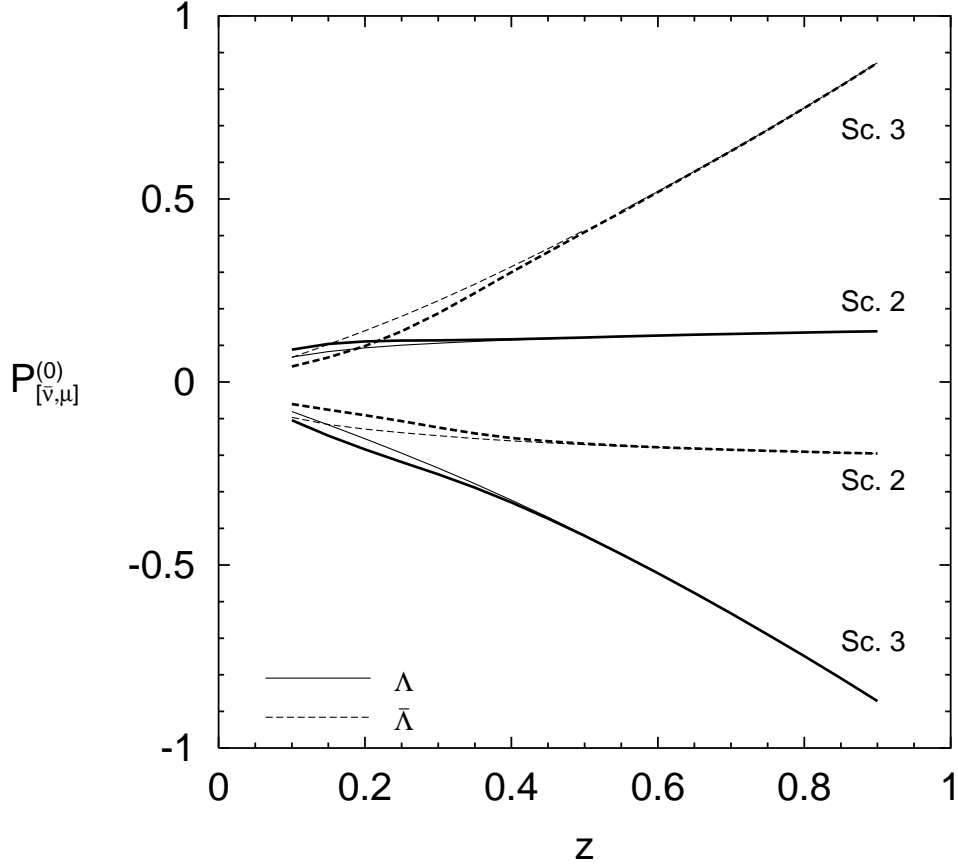


Figure 11: $P_{[;]}^{(0)}$ for Λ (solid lines) and $\bar{\Lambda}$ (dashed lines) hyperons, as a function of z , with a kinematical setup typical of NOMAD experiment at CERN (see Table 1 for details). Results are given for scenarios 2 and 3 of the polarized FF of Ref. [4]. Results with scenario 1 are almost negligible. Unpolarized (+) FF are from Ref. [4]; unpolarized GRV [14] partonic distributions have been used for the proton target. Estimates for $P_{[;]}^{(0)}$ are obtained from Eqs. (53) by using the corresponding results for $P_{[;]}^{(0)}$, shown in Fig. 2, and evaluating $T = d = d$ with the d , unpolarized FF of Ref. [9] (heavy lines) and Ref. [16] (thin lines); this last set has been modified by imposing SU(3) symmetry. The spread between the two corresponding sets of curves gives a good indication of the uncertainty due to the evaluation of the ratio T . Notice that this uncertainty is almost negligible for large z , where polarizations are expected to be sizeable for both scenarios 2 and 3.

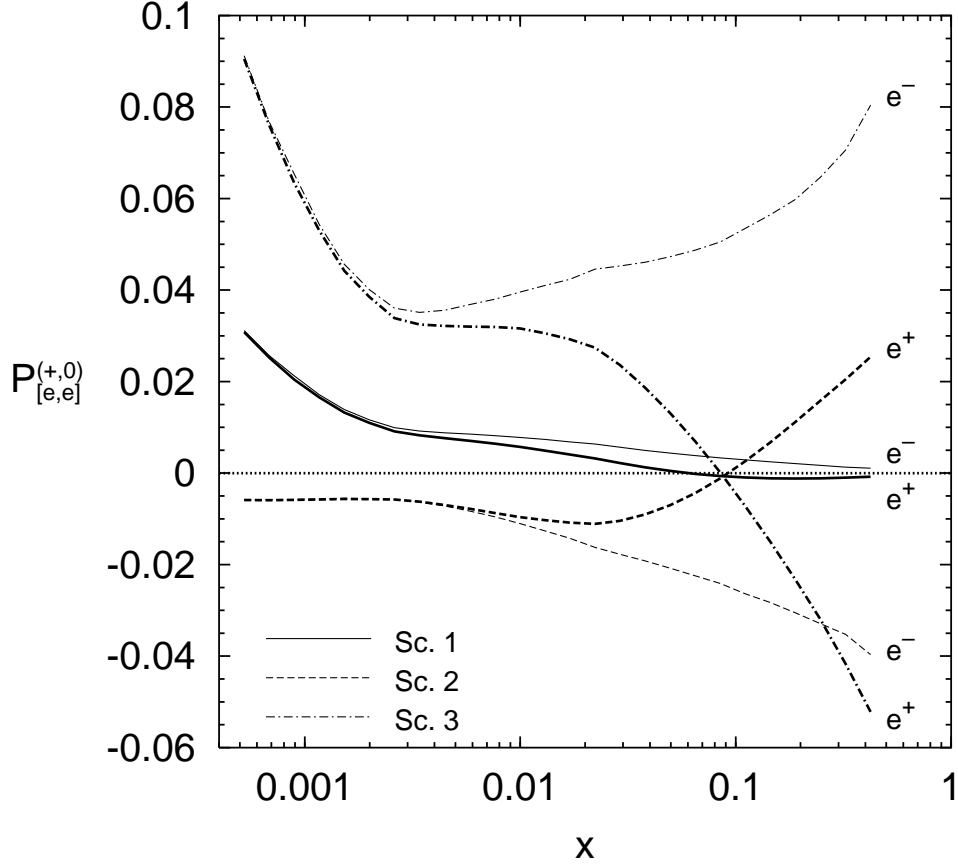


Figure 12: $P_{[e,e]}^{(+,0)}$ for hyperons, as a function of x , both for positron (heavy lines) and electron (thin lines) beams. The kinematical setup is typical of HERA experiments at DESY (see Table 1 for details). Results are given for all the three scenarios of the polarized FF of Ref. [4]. Unpolarized (+) FF are from Ref. [4]; unpolarized GRV [14] partonic distributions have been used for the proton target. Estimates for $P_{[e,e]}^{(+,0)}$ are obtained from Eqs. (53) by using the corresponding results for $P_{[e,e]}^{(+,0)}$, shown in Fig. 8, and evaluating $T = d = d$ with the unpolarized FF of Ref. [9]. The crossing at $x \approx 0.1$ for the case of positron beam is due to the interference between electromagnetic and weak contributions. Since $T = d = d$ is 1 at large x and becomes comparable to unity at very low x , we find, correspondingly, $P_{[e,e]}^{(+,0)} \approx P_{[e,e]}^{(+,0)}$ and $P_{[e,e]}^{(+,0)} \approx 2P_{[e,e]}^{(+,0)}$ (see text and Fig. 8 for more details).